communications materials

ARTICLE

https://doi.org/10.1038/s43246-021-00216-0 OPEN

Lithium-ion-conductive sulfide polymer electrolyte with disulfide bond-linked PS_4 tetrahedra for all-solid-state batteries

Atsutaka Kato [1✉], Mari Yamamoto[1], Futoshi Utsuno[2], Hiroyuki Higuchi[2] & Masanari Takahashi[1]

Due to their high conductivity and interface formability, sulfide electrolytes are attractive for use in high energy density all-solid-state batteries. However, electrode volume changes during charge-discharge cycling typically cause mechanical contact losses at the electrode/electrolyte interface, which leads to capacity fading. Here, to suppress this contact loss, isolated PS_4^{3-} anions are reacted with iodine to prepare a sulfide polymer electrolyte that forms a sticky gel during dispersion in anisole and drying of the resulting supernatant. This polymer, featuring flexible $(-P-S-S-)_n$ chains and enhanced solubility in anisole, is applied as a lithium-ion-conductive binder in sheet-type all-solid-state batteries, creating cells with low resistance and high capacity retention.

[1] Osaka Research Institute of Industrial Science and Technology, Morinomiya Center, 1-6-50, Morinomiya, Joto-ku, Osaka-city, Osaka 536-8553, Japan. [2] Idemitsu Kosan Co. Ltd., 1280, Kamiizumi, Sodegaura-city, Chiba 299-0293, Japan. ✉email: a-kato@omtri.or.jp

Since their commercialization in the 1990s, Li-ion batteries (LIBs) have been widely used in consumer electronics and have recently found large-scale energy storage applications in electric vehicles and smart grids[1–3]. However, the currently used LIBs contain flammable liquid organic electrolytes and therefore pose safety risks[4]. To mitigate these risks, one can replace organic liquid electrolytes with inorganic solid electrolytes, which feature higher thermal stability and are not susceptible to leakage[5]. This replacement affords high-energy-density all-solid-state batteries (ASSBs), which have attracted much attention, as exemplified by attempts to use solid electrolytes in combination with high-voltage cathodes[6,7], high-capacity sulfur electrodes[8,9], and Li metal anodes[10–13].

Among the various types of solid (e.g., sulfide-, oxide-, hydride-, and halide-based) electrolytes developed to date[5,14–16], the sulfide-based ones feature high conductivities and interface formability, and are therefore particularly well suited for ASSBs. In particular, sulfide electrolytes with $Li_{10}GeP_2S_{12}$-[17,18], argyrodite-[19,20], and $Li_7P_3S_{11}$-type[21,22] crystal structures have high conductivities ($>10^{-3}$ S cm^{-1}) comparable to those of liquid electrolytes. Sulfide electrolytes are easily deformed by pressing at room temperature[23], allowing one to form favorable electrode/electrolyte interfaces with high contact areas, and ensure sufficient ion conduction. However, the volume changes of the electrode active materials during charge/discharge induce local contact losses at ASSB electrode/electrolyte interfaces[24,25]. Typical sulfide electrolytes contain Li^+ ions and isolated anions such as PS_4^{3-}. Previously, sulfide polymers with $(-P-S-S-)_n$ units were predicted to electrochemically form at cathode/electrolyte interfaces during charging (delithiation)[26,27]. In contrast, thermodynamic calculations and structural analyses of the related interfaces indicate that such polymers undergo disproportionation into $P_2S_7^{4-}$ and elemental sulfur[28–30]. To date, no agreement has been reached, and the related discussions are still ongoing.

The improvement of existing processing technologies is vital for ASSB commercialization, with wet slurry coating recognized as a practical and scalable way of fabricating sheet-type ASSBs[31]. In this process, binders help to adhere the composites (containing the electrode active materials, solid electrolytes, and carbon-based conductive additives) to the current collector, make the composite sheets flexible, and allow roll-to-roll manufacturing. Both conventional LIBs and ASSBs use organic polymers, such as polyvinylidenefluoride[32], styrene-butadiene-styrene copolymers[33], and acrylonitrile-butadiene copolymers[34,35] as binders. However, the insulating nature of these binders hinders ionic and electronic conduction in ASSBs. To mitigate this problem, one can use volatile binders that can be thermally removed to afford binderless ASSBs[36]. Another strategy is to use Li^+-conductive polymer binders based on organic polymer electrolytes or hybrids of ionic liquid and organic polymer electrolytes[37–39]. Sulfide polymers will be a promising Li^+-conductive binder, and thus reduce hetero interfacial resistances in ASSBs.

Herein, we polymerized isolated PS_4^{3-} anions by reacting them with I_2 (Fig. 1). The reaction of two PS_4^{3-} anions with I_2 afforded a dimer comprising two PS_4 tetrahedra bridged with a disulfide (S–S) bond, whereas higher I_2 loadings afforded a potentially flexible chain polymer with a $(-P-S-S-)_n$ structure. We demonstrated the mechanochemical and liquid-phase syntheses of the sulfide polymer. This polymer was compared with previously reported structures like $P_2S_7^{4-}$ to provide useful suggestions for the design of cathode/electrolyte interfaces in ASSBs and was used as a binder in sheet-type ASSBs. LiI, a by-product of the above reaction, is also a Li-ion conductor[40] and can enhance the ionic conductivity of sulfide electrolytes[41,42] which suggests that sulfide polymer-LiI composites hold great promise as solid electrolytes.

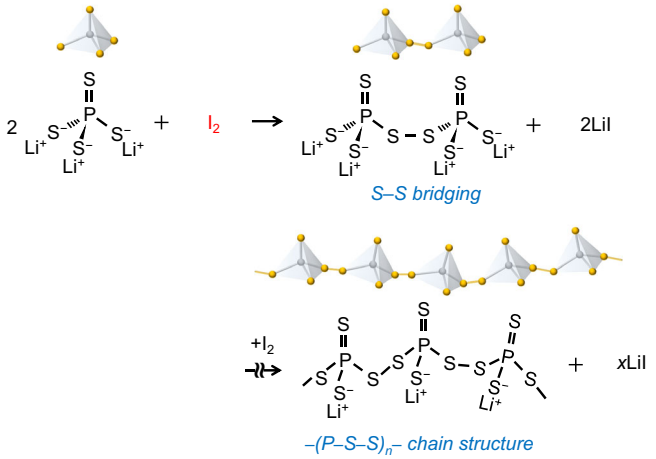

Fig. 1 Schematics of the I_2-induced polymerization of Li_3PS_4. The reaction of Li_3PS_4 with I_2 afforded a chain polymer with a $(-P-S-S-)_n$ structure.

Results

Mechanochemical synthesis of sulfide polymers and their characterization. Li_3PS_4 was prepared by ball milling a mixture of Li_2S and P_2S_5 and was further ball-milled with I_2 to afford sulfide polymers. We synthesized three kinds of sulfide polymers with different molar ratios; Li_3PS_4-I_2 (2:1), Li_3PS_4-I_2 (4:3), and Li_3PS_4-I_2 (1:1). Powder X-ray diffraction (PXRD) patterns acquired after the reaction with I_2 revealed the presence of LiI (PDF#01-075-5397) (Fig. 2(a)), and thus indicated the occurrence of Li_3PS_4 polymerization. The Raman spectrum of the amorphous polymerization product featured two main peaks at 477 and 390–420 cm^{-1} (Fig. 2(b)). The former peak, ascribed to S–S bond stretching, gained intensity with increasing I_2 loading, which reflected the concomitant increase in the extent of S–S cross-linking. Although elemental S exhibits a similar S–S stretching peak at 473 cm^{-1} [43], the peak at 477 cm^{-1} had a different origin, as it did not lose intensity after the polymer was washed with toluene to dissolve elemental S (Supplementary Fig. 1). The peak at 390–420 cm^{-1} was assigned to the stretching of P–S bonds and shifted to lower wavenumbers with increasing I_2 loading (cf. the P–S peak of pristine Li_3PS_4 at 421 cm^{-1}), which was ascribed to the progressive polymerization of Li_3PS_4 through S–S bridging. Supplementary Table 1 lists the Raman shifts of selected lithium thiophosphate anions[44–47], viz. $P_2S_7^{4-}$ (*pyro*-thiodiphosphate, two corner-sharing PS_4 tetrahedra), $P_2S_6^{4-}$ (*hypo*-thiodiphosphate with P–P bond), $P_2S_6^{2-}$ (*meta*-thiodiphosphate, two edge-sharing PS_4 tetrahedra), and PS_3^- (*meta*-thiophosphate, chain of corner-sharing PS_4 tetrahedra). The Raman shift of Li_3PS_4-I_2 (2:1), which featured two S–S bond-linked PS_4 tetrahedra ($P_2S_8^{4-}$) was similar to that of $P_2S_7^{4-}$, and that of Li_3PS_4-I_2 (1:1), which featured a chain structure (PS_4^-), was similar to that of PS_3^-. The structural difference between Li_3PS_4-I_2 polymers and the known anions of $P_2S_7^{4-}$ or PS_3^- is that in the former case, the PS_4 tetrahedra are linked through S–S bonds, whereas in the latter case, they share the corner S atoms. Because this difference is small, the corresponding Raman shifts were similar. Similar behavior has been reported for other thiophosphates such as Li_3PS_{4+n} and P_4S_{10+m}[48,49].

Li_3PS_4-I_2 (1:1) featured a particle size of 1–10 μm (Fig. 3(a)) and had good deformability (as did other sulfide electrolytes), affording a highly dense compact without clear original particle shapes after pressing at room temperature (Fig. 3(b)). The conductivities of Li_3PS_4-I_2 (2:1), (4:3), and (1:1) were 2.9×10^{-4}, 1.7×10^{-4}, and 3.0×10^{-5} S cm^{-1}, respectively, i.e., these values decreased with progressive polymerization (Fig. 3(c) and Supplementary Fig. 2).

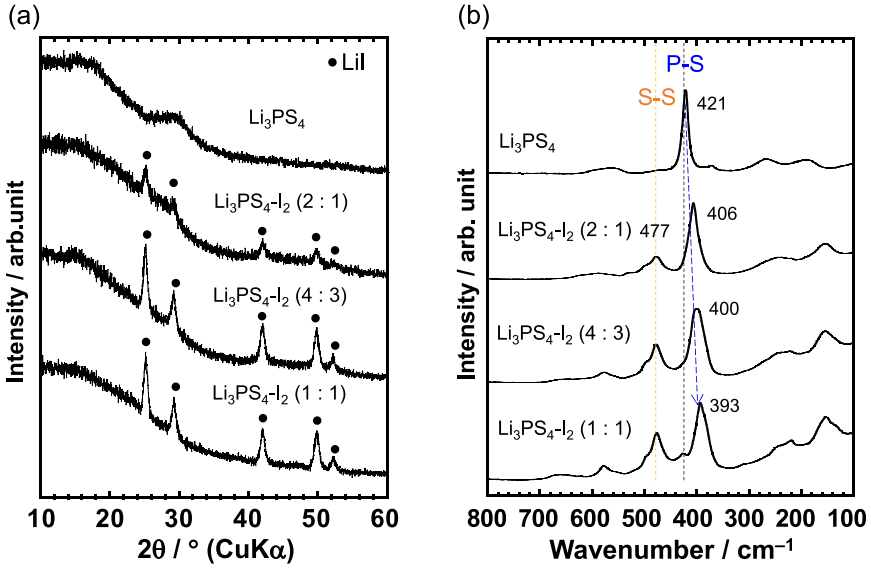

Fig. 2 Structural data for Li_3PS_4-I_2 polymers prepared by ball milling. a PXRD patterns and (**b**) Raman spectra. The diffraction peaks of cubic LiI are indicated with black circles.

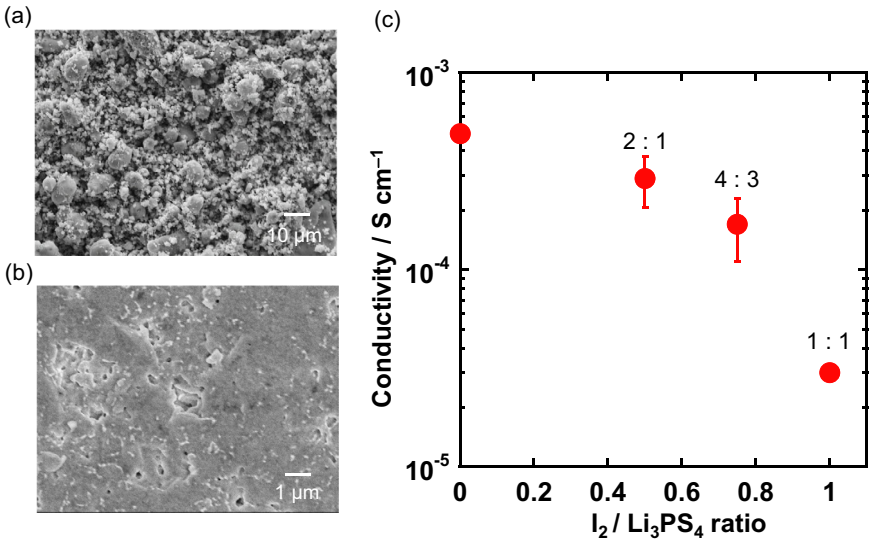

Fig. 3 Morphologies and ion-conduction behaviors of Li_3PS_4-I_2 polymers. SEM images of (**a**) the Li_3PS_4-I_2 (1:1) powder prepared by ball milling and (**b**) the fracture cross-section of the pellet prepared by cold-pressing the powders at 333 MPa. **c** Room temperature conductivities of Li_3PS_4-I_2 polymers. The error bar show standard deviation of Li_3PS_4-I_2 (2:1) for $n = 3$, Li_3PS_4-I_2 (4:3) for $n = 3$, and Li_3PS_4-I_2 (1:1) for $n = 5$, respectively.

Anisole, an aprotic solvent with a comparatively low donor number, is used as the binder solvent of sulfide electrolyte-based sheet-type ASSBs, as it does not attack these electrolytes[36]. Figure 4(a) shows that the solubility of Li_3PS_4-I_2 polymers in anisole increased with increasing I_2 loading and was highest for Li_3PS_4-I_2 (1:1). On the other hand, Li_2S-P_2S_5 solid electrolytes (*ortho*-, *pyro*-, and *meta*-thiophosphates) exhibited low solubility in anisole (Supplementary Fig. 3). Upon drying, the supernatant of the Li_3PS_4-I_2 (1:1) solution in anisole afforded a sticky gel, in line with the formation of long chains (Fig. 4(b)). The Raman spectrum of ball milling-prepared Li_3PS_4-I_2 (1:1) was compared with that of the dried supernatant of the corresponding anisole solution (Fig. 4(c)). Both the spectra featured similar S–S and P–S peaks around 477 and 390 cm^{-1}, respectively, indicating that these components were similar. However, the P–S peak of the ball milling-prepared Li_3PS_4-I_2 (1:1) was broader than that of the polymer recovered from the anisole solution, indicating that a greater variety of structures was formed in the former case. Figure 4(d) presents the ^{31}P NMR spectra of the two kinds of Li_3PS_4-I_2 (1:1) polymers, revealing the presence of three main peaks at 86–89, 100, and 120 ppm. The main peak at 86–89 ppm was tentatively assigned to the chain of disulfide-bond-linked PS_4 tetrahedra, whereas the other peaks could not be assigned. Supplementary Table 1 lists the ^{31}P NMR data for the known anions of lithium thiophosphates, revealing that a subpeak at ~120 ppm has been observed in the spectrum of PS_3^- [45]. The above unknown peaks may reflect the presence of branched structures or variable-size rings in addition to the regular chains of PS_4 tetrahedra, although further structural analysis is needed to reveal the details.

Liquid-phase synthesis of sulfide polymers. Li_3PS_4-I_2 polymers were also prepared by liquid-phase synthesis (LS), i.e., by stirring

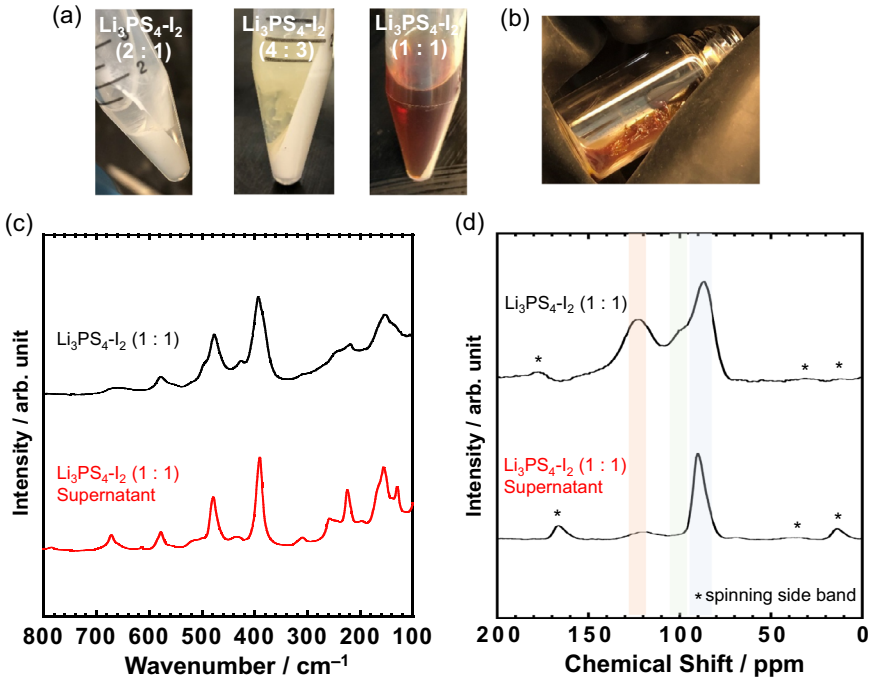

Fig. 4 Solubilities of ball milling-prepared Li_3PS_4-I_2 polymers in anisole. a Photographs of solutions of 10 wt% Li_3PS_4-I_2 (2:1), 20 wt% Li_3PS_4-I_2 (4:3), and 30 wt% Li_3PS_4-I_2 (1:1) in anisole after centrifugation at 2599 × *g*. **b** Photograph of the supernatant of the Li_3PS_4-I_2 (1:1) polymer solution during drying at 60 °C. **c** Raman and (**d**) ^{31}P NMR spectra of the Li_3PS_4-I_2 (1:1) polymer prepared by ball milling and the dried supernatant of its anisole solution.

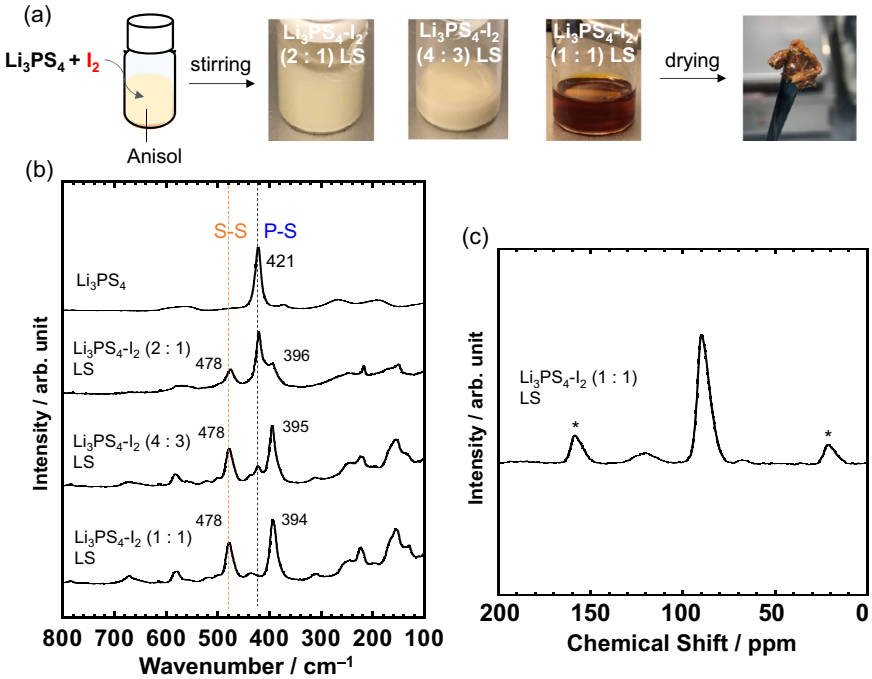

Fig. 5 Liquid-phase synthesis of Li_3PS_4-I_2 polymers. a Schematics of the synthetic process. Photographs of Li_3PS_4-I_2 polymer solutions obtained after stirring Li_3PS_4 and I_2 at 60 °C for one day. The Li_3PS_4-I_2 (1:1) polymer solution afforded a sticky gel upon drying. **b** Raman and (**c**) ^{31}P NMR spectra of Li_3PS_4-I_2 polymers prepared by liquid-phase synthesis.

Li_3PS_4 and I_2 in anisole at 60 °C for one day. In the case of Li_3PS_4-I_2 (1:1), the product was a clear brown solution at room temperature, while for Li_3PS_4-I_2 (2:1) and (4:3) (Fig. 5(a)), we observed precipitates that were identified as unreacted Li_3PS_4 based on their Raman spectra (Fig. 5(b)). Since I_2 is soluble in anisole, the polymerization of Li_3PS_4 progressed from the surface of the insoluble Li_3PS_4. As in the case of ball milling-prepared Li_3PS_4-I_2 (1:1), evaporation of the Li_3PS_4-I_2 (1:1) solution obtained after LS afforded a sticky gel, which contained hexagonal LiI (PDF#01-075-5395) (Supplementary Fig. 4). Notably, hexagonal LiI was also observed in the dried supernatant of the anisole solution of ball milling-prepared Li_3PS_4-I_2 (1:1). This hexagonal phase was reported to be metastable and undergo a slow structural change to the cubic phase even at room

temperature[50]. However, the fact that hexagonal LiI mainly precipitated upon the drying (at 60 °C) of Li_3PS_4-I_2 (1:1) polymers isolated from anisole solutions (the solution produced during LS and the supernatant obtained by dispersing ball milling–produced polymer) suggested that the sulfide polymer matrix prohibited the hexagonal-to-cubic transformation. The NMR spectrum of Li_3PS_4-I_2 (1:1) prepared by LS was similar to that of the dried supernatant of the anisole solution of the ball milling-prepared polymer, i.e., the Li_3PS_4-I_2 polymer with a $(–P–S–S–)_n$ chain structure could be also synthesized by LS. The conductivity of Li_3PS_4-I_2 (1:1) prepared by LS was 2.3×10^{-6} S cm^{-1} after drying at 200 °C (Supplementary Fig. 5), which was lower than the conductivity of ball milling-produced polymer.

Binder applications of sulfide polymers. The Li_3PS_4-I_2 polymer was used as a binder for ASSBs. Sheets containing Li_3PS_4 as a solid electrolyte were prepared by coating a slurry comprising this thiophosphate and ball milling-prepared Li_3PS_4-I_2 (1:1) (Fig. 6(a–c) and Supplementary Movie 1) in anisole. The obtained sheets with a thickness of ~80 μm could be bent around a 16-mm-diameter cylinder, although Li_3PS_4 powder was detached from the sheet in the absence of the binder. The conductivity of the Li_3PS_4 sheet with the sulfide polymer binder (2.3×10^{-4} S cm^{-1}, Supplementary Fig. 6) was close to that of the sheet without the binder (3.2×10^{-4} S cm^{-1}).

We also prepared composite electrode sheets (thickness: ~40 μm) comprising $LiNi_{1/3}Mn_{1/3}Co_{1/3}O_2$ (NMC), an argyrodite-type solid electrolyte (Li_6PS_5Cl with a conductivity of 2.2×10^{-3} S cm^{-1}), and Li_3PS_4-I_2 (1:1) as a binder (Supplementary Fig. 7) and evaluated the performance of the corresponding all-solid-state cell. We adopted the argyrodite-type solid electrolyte in the composite electrode due to its high ionic conductivity in the 10^{-3} S cm^{-1} range, ease of synthesis, and low costs of raw materials, which are advantageous for mass production[51,52]. As a result, typical charge-discharge curves of the NMC active material without obvious side reactions at 2.6–4.3 V (vs. Li/Li$^+$) were observed (Fig. 7(a)). The small cell resistance after the first charge indicated that the Li$^+$-conductive binder did not act as a resistive component (Fig. 7(b)). In addition, the above cell featured high cycling performance (Fig. 7(c)), retaining 93.8% of its capacity between cycles 5 and 200. These results suggest that the prepared Li_3PS_4-I_2 polymer can be used as an ion-conductive binder for sheet-type ASSBs.

Discussion

Herein, solid electrolytes prepared by I_2-induced polymerization of Li_3PS_4 were shown to contain S–S bridges, as indicated by the Raman peak at 477 cm^{-1}. This peak was retained after the polymer was washed with toluene to remove elemental sulfur and thus truly originated from the S–S linkages in the polymer. The solubility of the sulfide polymer in anisole increased with increasing I_2 loading, which was in contrast with the low solubilities of *ortho*-, *pyro*-, and *meta*-thiophosphate Li_2S-P_2S_5 electrolytes. The formation of a sticky gel upon the drying of the Li_3PS_4-I_2 (1:1) solution was in line with the formation of chain structures. Notably, the sulfide polymer did not undergo disproportionation into the known thiophosphates and elemental S and was assumed to contain PS_4 tetrahedra cross-linked with S–S bonds. On the other hand, the sulfide polymer was similar to the known thiophosphates with corner-sharing PS_4 tetrahedra in terms of the Raman shifts of P–S bonds and ^{31}P NMR shifts, which indicated the similarity between the chemical environments of P atoms. The same behavior has been observed in reports on the structural analysis of cathode/electrolyte interfaces[29,53]. Further structural analyses of the sulfide polymer are expected to provide critical insights into the related cathode/electrolyte interfaces to facilitate their design in ASSBs.

Liquid-phase synthesis is well suited for mass production[54]. The sulfide polymer could be prepared by both liquid-phase and mechanochemical syntheses, although the sulfide polymers prepared by liquid-phase possessed lower conductivities. The polymer structure and the composite state with LiI would influence the conductivities of sulfide polymers. LiI is a poor ionic conductor[40], however, doping it can improve the conductivity of

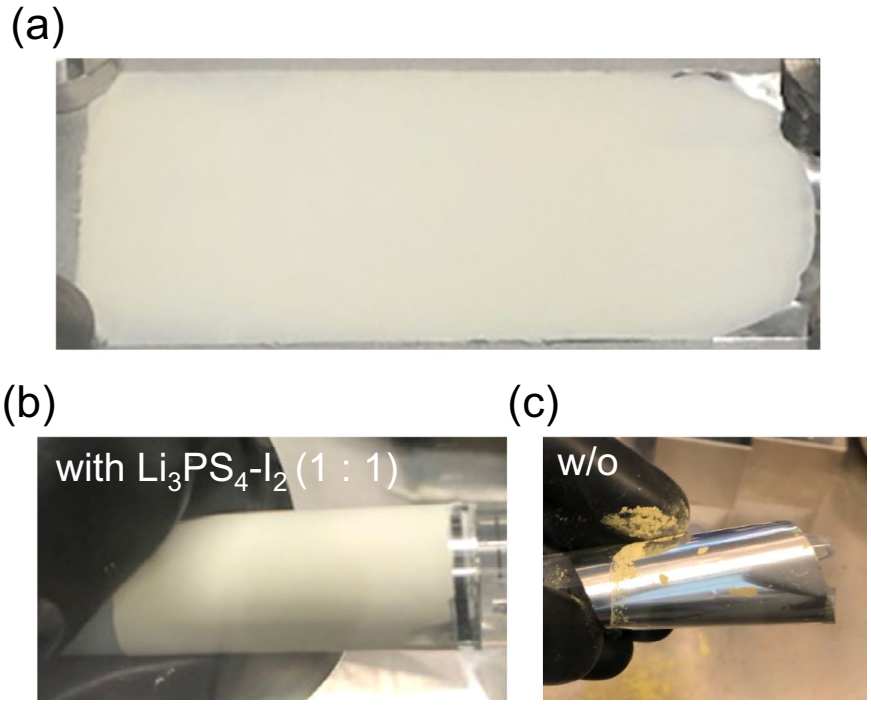

Fig. 6 Sheets of Li_3PS_4 solid electrolytes prepared by wet slurry coating. a Appearance of the sheet prepared using the Li_3PS_4-I_2 (1:1) polymer as a binder. The results of bending around a 16-mm-diameter cylinder are displayed for sheets prepared (**b**) with and (**c**) without the binder.

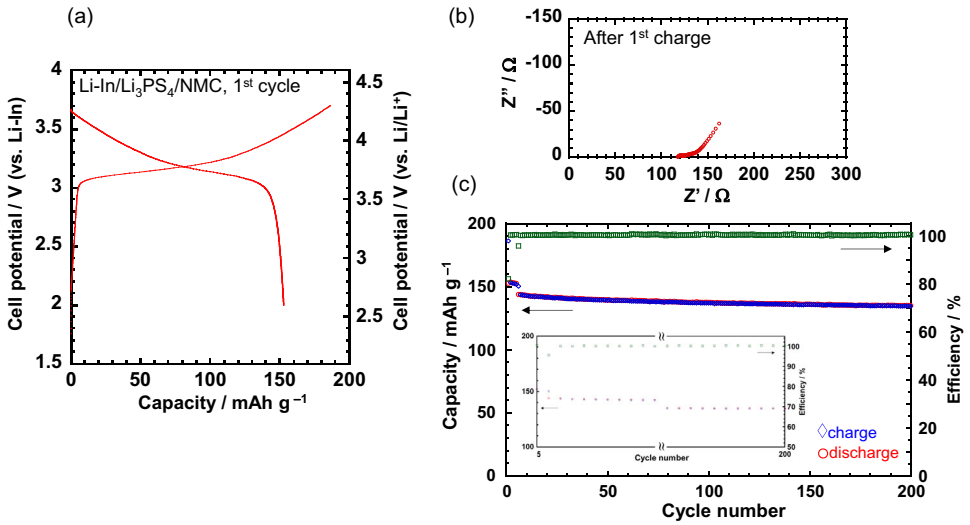

Fig. 7 Electrochemical performance of an all-solid-state cell containing Li_3PS_4-I_2 (1:1) as a polymer binder. a First charge-discharge curve, **b** Nyquist plot after first charge, and (**c**) cycling performance of an all-solid-state Li-In/Li_3PS_4/NMC cell containing Li_3PS_4-I_2 (1:1) as a polymer binder. The inset displays the enlarged view at the beginning and end of ten cycles.

sulfide electrolytes[41,42]. Although LiI crystal was observed in the XRD patterns, some amount of LiI were considered to be doped in the amorphous sulfide polymers and enhance the conductivities. The ball milling process was assumed to increase doped-LiI in the sulfide polymer, and made the higher conductivity. Removing redundant LiI crystal with poor ionic conductivity and increasing doped-LiI will improve the conductivities of sulfide polymers. The sulfide polymer was used as a binder to prepare sheets comprising Li_3PS_4 and NMC composites as solid electrolytes. These sheets were bendable, and all-solid-state cells containing NMC composite sheets exhibited low resistance and high capacity retention. The NMC loading (~2 mg) was low compared to the practical value, and it was difficult to prepare thick electrode sheets with >100 μm thickness without cracking. Further works such as designing a molecular weight and a structure of the sulfide polymer will improve the adhesiveness of the binder. Thus, the flexible and ionically conductive sulfide polymer prepared herein is expected to facilitate the development of more robust electrode/electrolyte interfaces in ASSBs.

Methods

Material synthesis. Solid electrolytes were prepared by ball milling appropriate amounts of Li_2S (Furuuchi Chemical Corp.) and P_2S_5 (Sigma-Aldrich) at 500 rpm for 20 h using ZrO_2 pots (volume: 45 mL) and balls (diameter: 5 mm). The thus obtained Li_3PS_4 was polymerized by ball milling with I_2 (Kojundo Chemical Lab. Co.) at 500 rpm for 20 h. Dehydrated heptane (Fujifilm Wako Pure Chemical Corp.) was added in the pots with the starting materials as a medium for ball milling. The heptane medium was removed after ball milling by drying the samples at room temperature. The extent of S–S bridging was determined by I_2 loading. The I_2-induced polymerization of Li_3PS_4 and I_2 was also carried out by one-day stirring in anisole at 60 °C and a total solid content of 25 wt%. The resulting Li_3PS_4-I_2 polymer solution was dried in a vacuum at 60 °C. All the samples were synthesized in a dry Ar atmosphere.

Material characterization. PXRD patterns (SmartLab, Rigaku; Cu K_α radiation, $2\theta = 10-60°$, step = 0.02°) were recorded in sealed vessels under dry Ar. Raman spectra (LabRAM HR Evolution, HORIBA) were recorded in the wavenumber range 100–800 cm^{-1} using an exposure of 1 s 30 times and an excitation laser with a wavelength of 532 nm. For Raman measurements, the samples were sealed in glass tubes filled with dry Ar. Solid-state magic-angle-spinning ^{31}P NMR (ECZ400R, JEOL) measurements were performed at a spinning speed of 12 kHz. The powdered samples were sealed in spinners in a dry Ar-filled glove box. A 90° 3.8 μs pulse with a recycle delay of 300 s was used, and the observed frequency was 161.944 MHz. Powder morphologies and pellet fracture cross-sections were examined by scanning electron microscopy (SEM; JSM-7800F, JEOL). Sample pellets were prepared by pressing the powders at 333 MPa and room temperature. All SEM samples were prepared in a dry Ar-filled glove box and transferred in sealed vessels.

Preparation of solid electrolyte and electrode composite sheets. The Li_3PS_4-I_2 (1:1) polymer synthesized by ball milling was used as a binder. Solid electrolyte sheets were prepared by mixing Li_3PS_4 powders with the Li_3PS_4-I_2 (1:1) polymer in anisole in a weight ratio of 95:5 followed by coating on Al current collector sheets. Electrode composite sheets were also prepared by coating slurries of $LiNbO_3$-coated $LiNi_{1/3}Co_{1/3}Mn_{1/3}O_2$ (NMC; active material)[55], argyrodite-type Li_6PS_5Cl (solid electrolyte)[56,57], acetylene black, and the Li_3PS_4-I_2 (1:1) polymer in anisole (70:30:5:5, w/w/w/w) on Al current collector sheets. The sheets were dried at 60 °C in a dry Ar atmosphere overnight and further dried in a vacuum at 160 °C for 3 h.

Conductivity measurements. Powders or sheets were put into a polyimide tube with a diameter of 10 mm and sandwiched between two stainless steel rods as an ion-blocking electrode. The cells were pressed at 333 MPa, and conductivities were measured at least three times at room temperature using an AC impedance analyzer (cell test system 1470E, Solartron Analytical; lead wires connected to stainless steel rods) in the frequency range from 10 Hz to 1 MHz. All procedures were conducted under dry Ar.

All-solid-state cell assembly and electrochemical measurements. NMC composite sheets (NMC loading = ~2 mg) punched into circles with a diameter of 9.5 mm and a Li_3PS_4 separator layer (80 mg) were put into a polyimide tube (10 mm in diameter) and pressed together at 296 MPa. A Li-In alloy foil (Li foil: thickness 0.2 mm, diameter 4 mm, and In foil: thickness 0.1 mm, diameter 8 mm) was placed on the surface of the separator side of the bilayer pellet as a counter electrode. The three-layered pellet was sandwiched between two stainless steel rods as a current collector, and a pressure of 111 MPa was applied to assemble the cell. All processes were performed in a dry Ar-filled glove box (DBO-2NKP, Miwa Manufacturing Co., Ltd.). Charge-discharge tests were carried out at 0.071 mA cm^{-2} in the first five cycles and at 0.14 mA cm^{-2} in the subsequent cycles at 30 °C under dry Ar using an electrochemical measurement device (BTS-2004, Nagano Co.). Cell resistance was measured after the first charge using an AC impedance analyzer (cell test system 1470E, Solartron Analytical). The cells were uniaxially pressed under 75 MPa during the electrochemical measurements.

Data availability

The datasets that support the findings of this study are available from the corresponding authors upon reasonable request.

Received: 10 February 2021; Accepted: 15 October 2021;
Published online: 09 November 2021

References

1. Ding, Y., Cano, Z. P., Yu, A., Lu, J. & Chen, Z. Automotive Li-Ion batteries: current status and future perspectives. *Electrochem. Energ. Rev.* **2**, 1–28 (2019).
2. Dunn, B., Kamath, H. & Tarascon, J. M. Electrical energy storage for the grid: a battery of choices. *Science* **334**, 928–935 (2011).
3. Hesse, H. C., Schimpe, M., Kucevic, D. & Jossen, A. Lithium-ion battery storage for the grid - A review of stationary battery storage system design tailored for applications in modern power grids. *Energies.* **10**, 2107 (2017).
4. Mauger, A. & Julien, C. M. Critical review on lithium-ion batteries: are they safe? Sustainable? *Ionics* **23**, 1933–1947 (2017).
5. Manthiram, A., Yu, X. & Wang, S. Lithium battery chemistries enabled by solid-state electrolytes. *Nat. Rev. Mater.* **2**, 16103 (2017).
6. Oh, G., Hirayama, M., Kwon, O., Suzuki, K. & Kanno, R. Bulk-type all solid-state batteries with 5 V Class LiNi0.5Mn1.5O4 cathode and Li10GeP2S12 solid electrolyte. *Chem. Mater.* **28**, 2634–2640 (2016).
7. Yubuchi, S., Ito, Y., Matsuyama, T., Hayashi, A. & Tatsumisago, M. 5 v class LiNi0.5Mn1.5O4 positive electrode coated with Li3PO4 thin film for all-solid-state batteries using sulfide solid electrolyte. *Solid State Ionics* **285**, 79–82 (2016).
8. Bonnick, P. & Muldoon, J. The Dr Jekyll and Mr Hyde of lithium sulfur batteries. *Energy Environ. Sci.* **13**, 4808–4833 (2020).
9. Nagao, M., Hayashi, A. & Tatsumisago, M. Sulfur–carbon composite electrode for all-solid-state Li/S battery with Li2S–P2S5 solid electrolyte. *Electrochim. Acta* **56**, 6055–6059 (2011).
10. Hatzell, K. B. et al. Challenges in lithium metal anodes for solid-state batteries. *ACS Energy Lett.* **5**, 922–934 (2020).
11. Zhao, F. et al. Ultrastable anode interface achieved by fluorinating electrolytes for all-solid-state Li metal batteries. *ACS Energy Lett.* **5**, 1035–1043 (2020).
12. Lee, Y. G. et al. High-energy long-cycling all-solid-state lithium metal batteries enabled by silver–carbon composite anodes. *Nat. Energy* **5**, 299–308 (2020).
13. Hitz, G. T. et al. High-rate lithium cycling in a scalable trilayer Li-garnet-electrolyte architecture. *Mater. Today* **22**, 50–57 (2019).
14. Zhang, Z. et al. New horizons for inorganic solid state ion conductors. *Energy Environ. Sci.* **11**, 1945–1976 (2018).
15. Li, X. et al. Progress and perspectives on halide lithium conductors for all-solid-state lithium batteries. *Energy Environ. Sci.* **13**, 1429–1461 (2020).
16. Wu, J. et al. Lithium/sulfide all-solid-state batteries using sulfide electrolytes. *Adv. Mater.* **33**, 2000751 (2021).
17. Kamaya, N. et al. A lithium superionic conductor. *Nat. Mater.* **10**, 682–686 (2011).
18. Kato, Y. et al. High-power all-solid-state batteries using sulfide superionic conductors. *Nat. Energy* **1**, 16030 (2016).
19. Rao, R. P. & Adams, S. Studies of lithium argyrodite solid electrolytes for all-solid-state batteries. *Phys. Status Solidi A* **208**, 1804–1807 (2011).
20. Zhou, L., Assoud, A., Zhang, Q., Wu, X. & Nazar, L. F. New family of argyrodite thioantimonate lithium superionic conductors. *J. Am. Chem. Soc.* **141**, 19002–19013 (2019).
21. Yamane, H. et al. Crystal structure of a superionic conductor, Li7P3S11. *Solid State Ionics* **178**, 1163–1167 (2007).
22. Seino, Y., Ota, T., Takada, K., Hayashi, A. & Tatsumisago, M. A sulphide lithium super ion conductor is superior to liquid ion conductors for use in rechargeable batteries. *Energy Environ. Sci.* **7**, 627–631 (2014).
23. Sakuda, A., Hayashi, A. & Tatsumisago, M. Sulfide solid electrolyte with favorable mechanical property for all-solid-state lithium battery. *Sci. Rep.* **3**, 2261 (2013).
24. Koerver, R. et al. Capacity fade in solid-state batteries: interphase formation and chemomechanical processes in nickel-rich layered oxide cathodes and lithium thiophosphate solid electrolytes. *Chem. Mater.* **29**, 5574–5582 (2017).
25. Shi, T. et al. Characterization of mechanical degradation in an all-solid-state battery cathode. *J. Mater. Chem. A* **8**, 17399–17404 (2020).
26. Sumita, M., Tanaka, Y. & Ohno, T. Possible polymerization of PS4 at a Li3PS4/FePO4 interface with reduction of the FePO4 phase. *J. Phys. Chem. C* **121**, 9698–9704 (2017).
27. Hakari, T. et al. Structural and electronic-state changes of a sulfide solid electrolyte during the Li Deinsertion-insertion processes. *Chem. Mater.* **29**, 4768–4774 (2017).
28. Koerver, R. et al. Redox-active cathode interphases in solid-state batteries. *J. Mater. Chem. A* **5**, 22750–22760 (2017).
29. Schwietert, T. K. et al. Clarifying the relationship between redox activity and electrochemical stability in solid electrolytes. *Nat. Mater.* **19**, 428–435 (2020).
30. Richards, W. D., Miara, L. J., Wang, Y., Kim, J. C. & Ceder, G. Interface stability in solid-state batteries. *Chem. Mater.* **28**, 266–273 (2016).
31. Tan, D. H. S., Banerjee, A., Chen, Z. & Meng, Y. S. From nanoscale interface characterization to sustainable energy storage using all-solid-state batteries. *Nat. Nanotechnol.* **15**, 170–180 (2020).
32. Zhang, X. et al. Synergistic coupling between Li6.75La3Zr1.75Ta0.25O12 and poly(vinylidene fluoride) induces high ionic conductivity, mechanical strength, and thermal stability of solid composite electrolytes. *J. Am. Chem. Soc.* **139**, 13779–13785 (2017).
33. Sakuda, A. et al. All-solid-state battery electrode sheets prepared by a slurry coating process. *J. Electrochem. Soc.* **164**, A2474–A2478 (2017).
34. Riphaus, N. et al. Slurry-based processing of solid electrolytes: a comparative binder study. *J. Electrochem. Soc.* **165**, A3993–A3999 (2018).
35. Nam, Y. J., Oh, D. Y., Jung, S. H. & Jung, Y. S. Toward practical all-solid-state lithium-ion batteries with high energy density and safety: Comparative study for electrodes fabricated by dry- and slurry-mixing processes. *J. Power Sources* **375**, 93–101 (2018).
36. Yamamoto, M., Terauchi, Y., Sakuda, A. & Takahashi, M. Binder-free sheet-type all-solid-state batteries with enhanced rate capabilities and high energy densities. *Sci. Rep.* **8**, 1212 (2018).
37. Kim, K. T. et al. Tailoring Slurries Using Cosolvents and Li Salt Targeting Practical All-Solid-State Batteries Employing Sulfide Solid Electrolytes. *Adv. Energy Mater.* **11**, 2003766 (2021).
38. Oh, D. Y. et al. Slurry-fabricable Li + -Conductive polymeric binders for practical all-solid-state lithium-ion batteries enabled by solvate ionic liquids. *Adv. Energy Mater.* **9**, 1–10 (2019).
39. Cho, W., Park, J., Kim, K., Yu, J. S. & Jeong, G. Sulfide-compatible conductive and adhesive glue-like interphase engineering for sheet-type all-solid-state battery. *Small.* **17**, e1902138 (2019).
40. Liang, C. C. Conduction characteristics of the lithium iodide-aluminum oxide solid electrolytes. *J. Electrochem. Soc.* **120**, 1289 (1973).
41. Mercier, R., Malugani, J. P., Fahys, B. & Robert, G. Superionic conduction in Li2S - P2S5 – LiI - glasses. *Solid State Ionics* **5**, 663–666 (1981).
42. Wu, L. et al. Superior lithium-stable Li7P2S8I solid electrolyte for all-solid-state lithium batteries. *J. Power Sources* **491**, 229565 (2021).
43. Nims, C., Cron, B., Wetherington, M., Macalady, J. & Cosmidis, J. Low frequency Raman Spectroscopy for micron-scale and in vivo characterization of elemental sulfur in microbial samples. *Sci. Rep.* **9**, 7971 (2019).
44. Tachez, M., Malugani, J. P., Mercier, R. & Robert, G. Ionic conductivity of and phase transition in lithium thiophosphate Li3PS4. *Solid State Ionics* **14**, 181–185 (1984).
45. Dietrich, C. et al. Lithium ion conductivity in Li2S–P2S5 glasses – Building units and local structure evolution during the crystallization of superionic conductors Li3PS4, Li7P3S11 and Li4P2S7. *J. Mater. Chem. A* **5**, 18111–18119 (2017).
46. Dietrich, C. et al. Synthesis, structural characterization, and lithium ion conductivity of the lithium thiophosphate Li2P2S6. *Inorg. Chem.* **56**, 6681–6687 (2017).
47. Dietrich, C. et al. Spectroscopic characterization of lithium thiophosphates by XPS and XAS – a model to help monitor interfacial reactions in all-solid-state batteries. *Phys. Chem. Chem. Phys.* **20**, 20088–20095 (2018).
48. Lin, Z., Liu, Z., Fu, W., Dudney, N. J. & Liang, C. Lithium polysulfidophosphates: a family of lithium-conducting sulfur-rich compounds for lithium-sulfur batteries. *Angew. Chem. Int. Engl.* **52**, 7460–7463 (2013).
49. Li, X. et al. Sulfur-rich phosphorus sulfide molecules for use in rechargeable lithium batteries. *Angew. Chem. Int. Engl.* **56**, 2937–2941 (2017).
50. Wassermann, B., Hönle, W. & Martin, T. P. Hexagonal LiI. *Solid State Commun.* **65**, 561–564 (1988).
51. Yu, C., Zhao, F., Luo, J., Zhang, L. & Sun, X. Recent development of lithium argyrodite solid-state electrolytes for solid-state batteries: synthesis, structure, stability and dynamics. *Nano Energy* **83**, 105858 (2021).
52. Boulineau, S., Courty, M., Tarascon, J. M. & Viallet, V. Mechanochemical synthesis of Li-Argyrodite Li6PS5X (X = Cl, Br, I) as sulfur-based solid electrolytes for all solid state batteries application. *Solid State Ionics* **221**, 1–5 (2012).
53. Dewald, G. F. et al. Experimental assessment of the practical oxidative stability of lithium thiophosphate solid electrolytes. *Chem. Mater.* **31**, 8328–8337 (2019).
54. Miura, A. et al. Liquid-phase syntheses of sulfide electrolytes for all-solid-state lithium battery. *Nat. Rev. Chem.* **3**, 189–198 (2019).
55. Ohta, N. et al. LiNbO3-coated LiCoO2 as cathode material for all solid-state lithium secondary batteries. *Electrochem. Commun.* **9**, 1486–1490 (2007).
56. Yu, C., van Eijck, L., Ganapathy, S. & Wagemaker, M. Synthesis, structure and electrochemical performance of the argyrodite Li6PS5Cl solid electrolyte for Li-ion solid state batteries. *Electrochim. Acta* **215**, 93–99 (2016).
57. Yu, C. et al. Facile synthesis toward the optimal structure-conductivity characteristics of the argyrodite Li6PS5Cl solid-state electrolyte. *ACS Appl. Mater. Interfaces* **10**, 33296–33306 (2018).

Acknowledgements

This work was financially supported by JSPS KAKENHI (Grant No. JP19K21108).

Author contributions

A.K. proposed the concept of this work, wrote the manuscript, and collected the experimental data except for NMR measurements. F.U. and H.H. recorded NMR spectra. M.Y. contributed to result analysis. A.K., F.U., H.H., and M.T. supervised the research. All authors discussed the results and commented on the manuscript.

Competing interests

F.U. and H.H. are employed by Idemitsu Kosan Co. Ltd. The other authors declare no competing interests.

Additional information

Supplementary information The online version contains supplementary material available at https://doi.org/10.1038/s43246-021-00216-0.

Correspondence and requests for materials should be addressed to Atsutaka Kato.

Peer review information *Communications Materials* thanks Yoon Seok Jung and the other, anonymous, reviewer(s) for their contribution to the peer review of this work. Primary Handling Editor: John Plummer.

Reprints and permission information is available at http://www.nature.com/reprints

Publisher's note Springer Nature remains neutral with regard to jurisdictional claims in published maps and institutional affiliations.